Journal of Sol-Gel Science and Technology 24, 69–80, 2002
© 2002 Kluwer Academic Publishers. Manufactured in The Netherlands.

Characterization of V-MCM-41 Mesoporous Materials

DER-SHING LEE*AND TSUNG-KWEI LIU
Department of Geosciences, National Taiwan University, Taipei 106, Taiwan
ipo02022@mail.moeaipo.gov.tw

Received May 29, 2001; Accepted January 9, 2002

Abstract. A series of vanadosilicate V-MCM-41 mesoporous materials with various compositions have been synthesized using vanadium sulfate as the source of vanadium. Hexadecyltrimethylammonium bromide was used as a surfactant in the synthesis. The samples were characterized with nitrogen sorption, X-ray diffraction, framework FTIR, diffuse reflectance UV-visible spectroscopy, differential thermal analysis, thermogravimetric analysis, scanning electron microscopy and transmission electron microscopy. The results show that the solid products had the MCM-41 structure and contained only atomically dispersed vanadium consistent with framework vanadium in V-MCM-41. N_2 sorption measurements and TEM demonstrated the high mesoporosity of V-MCM-41. The incorporation of vanadium into MCM-41 decreased the surface area to some extent. The morphology of V-MCM-41 was plate with stepped and smooth surfaces. TEM reveals a regular hexagonal array of uniform channels with curved and rectilinear morphologies. The hexagonal array structure of uniform pore size was observed by TEM. It is proved that the pores were highly aligned.

Keywords: mesoporous molecular sieve, MCM-41, zeolite, vanadium-containing molecular sieve

Introduction

Since the discovery of the mesoporous molecular sieves [1, 2], many researchers have focused on this material [3–10]. One form of this series, MCM-41, which possessed a uniform arrangement of hexagonal shape mesopores of diameter varying from 15 to 100 Å, have received great attention in material science and catalysis. MCM-41 is of particular interest because it has two important roles. Its narrow pore size distribution and straight, unconnected channels make it an ideal model adsorbent for fundamental theoretical studies of fluid behavior in confined regions [9–27]. Its large and controllable pore size enables it to host large molecule than alternative catalytic materials, bringing it into the size range required for hosting biological materials [4].

Isomorphous substitution of silicon with other elements is an excellent strategy in creating active sites and anchoring sites for active molecules in the design of new heterogeneous catalyst. Many metals, such as aluminum, titanium, manganese, iron, boron, niobium and vanadium, have been incorporated into the framework of MCM-41 [6, 16, 17, 28–38]. V-zeolites and V-MCM-41 are remarkable catalysts for the selective oxidation of organic molecules. Their large surface area made it possible to disperse a large number of catalytic active vanadium centers. In turn, their narrow pore size distribution installed a high selectivity in their catalytic properties, allowing only molecules able to diffuse into their channels to be transformed. For V-zeolites, catalytic activity was generally limited molecules with a kinetic diameter lower than ca. 0.65 nm. For V-MCM-41, however, the transformation of large organic molecules becomes possible. The established importance of vanadium compounds as oxidation catalysts have made the introduction of vanadium into the MCM-41 structure particularly desirable. It is expected that the catalytic properties of

*To whom all correspondence should be addressed.

V-MCM-41 are dependent on the location of vanadium and the concentration of vanadium in the MCM-41 structure. However, incorporation of transition metal cations in the framework of pure silica polymorphs of zeolites is not always easy and has some limited amount. Several research groups have attempted to incorporate vanadium into MCM-41. The direct hydrothermal synthesis of vanadium-substituted MCM-41 was first achieved by Reddy et al. [30, 31]. The sample obtained by hydrothermal synthesis contained dispersed vanadium center. Gontier et al. [39] observed that vanadium cations in synthetic V-MCM-41 were probably in a coordination state like those in aqueous solution. Morey et al. [28] prepared the mesoporous material V-MCM-48 using an impregnation method. By UV-visible spectroscopy measurement they suggested that the hydroxyl group on the wall of the MCM-48 were employed as anchoring sites of vanadium to form pesudooctahedral $O_{3/2}$ V═O graft on the mesoporous wall. Park et al. [40] reported that V-MCM-41 are present in the chemical environment of octahedral and octahedral vanadium is decreased and tetrahedral vanadium is increased inversely with raising the calcination temperature. The best quality XRD pattern of the product of Si/V = 27 was attributed to heterogeneous nucleation mechanism. V-MCM-41 having the Si/V ratio lower than 20 were completely collapsed after calcination. Chao et al. [41] reported that vanadium could be incorporated in the tubular wall of MCM-41 through interaction with surface silanol groups. Upon calcination and exposure to air, a thin film of vanadate is uniformly deposited on the wall-surface of MCM-41 support. Spectroscopic characterization of V-MCM-41 obtained by the hydrothermal method describing two different sites of anchoring for vanadium was presented by Luan et al. [42, 43] and Lu and Chen [16]. Wei et al. [44] reported that vanadium is incorporated into the framework of hydrated and dehydrated samples, mostly occupying isolated tetrahedral sites. A small portion of octahedral sites involving water coordination were observed in hydrated samples with large pore size. The higher hydrophobicity of the vanadium local environment was obtained from smaller pore size V-MCM-41 catalyst. They [45] also reported that a strong effect of pore size of V-MCM-41 on the catalytic activity of methanol oxidation was observed in the form of volcano curve and can be correlated with a variation in the local bond angle of Si─O─V. Lin and Haller [46] reported that the active sites for gas phase methanol oxidation on V-MCM-41 was weak Lewis acid site, which has an isolated tetrahedral coordination of vanadium with surrounding oxygen anions. V-MCM-41 is a stable catalyst against gas phase methanol oxidation at 350°C. The saturation value of vanadium concentration in this catalytic system was 0.41 wt%, and produces a very stable isolated tetrahedral coordination V site. Chatterjee et al. [47] developed a method to synthesize V-MCM-41 at room temperature using a minimum amount of template. The increase of unit cell parameter and decrease of Q_3/Q_4 ratio of ^{29}Si NMR spectra with vanadium content suggest the incorporation of vanadium in the framework of the MCM-41 structure. UV-vis and ^{51}V NMR studies confirmed the presence of V^{5+} ion in the tetrahedral position. In the case of a freshly synthesized sample, VO^{2+} in a square pyramidal arrangement was detected by ESR. After calcination, V^{5+} species remain in the tetrahedral arrangement. Grubert et al. [48] used hydrothermal synthesis, impregnation and chemical vapor deposition methods to prepare V-MCM-41. In all cases the vanadium species were found to be located almost completely inside the pore system of the support in more-or-less distorted tetrahedral coordination in the dehydrated state. Most of vanadium is distributed mononuclearly, but impregnation and especially chemical vapor deposition resulted additionally in the formation of some chain-like oligomeric vanadium oxide clusters. Arnold et al. [49] reported that the vanadium content of V-MCM-41 was dependent not only on the amount of vanadiul sulfate, but also in the sequence of addition of the gel components and the presence of alkali metal chlorides. A direct evidence of vanadium species in tetrahedral and octahedral coordination in V-MCM-41 was recently characterized by UV resonance Raman bands at 1070 and 930 cm^{-1} [50]. In general, three forms of vanadium species, isolated tetrahedral, two-dimensional octahedral species and crystalline V_2O_5, are believed to be present. It is believed that the presence of these species is dependent on the concentration of vanadium and preparation method.

A series of mesoporous vandosilicate V-MCM-41 materials with various compositions have been synthesized in this study. The materials were characterized with X-ray diffraction (XRD), framework FTIR, diffuse reflectance UV-visible spectroscopy (UV-vis), nitrogen adsorption-desorption measurement, scanning electron microscopy (SEM), transmission electron microscopy (TEM), thermogravimetric analysis (TGA) and differential thermal analysis (DTA).

Experimental

Chemicals

Sodium silicate was purchased from Showa Chemicals Co., Japan. Vanadium(IV) oxidsulfat pentahydrate ($VOSO_4 \cdot 5H_2O$) were given by Merck. Hexadecyltrimethylammonium bromide (C_{16}TMABr) was purchased from Aldrich. All chemicals were used without further purification.

Synthesis

A series of V-MCM-41 samples with various compositions was synthesized. The molar composition of the gel for the sample with Si:V = 100:2 is 1 SiO_2:0.5 C_{16}TMABr:0.4627 Na_2O:0.02 VO_2:0.005: 2.0314H_2O. The typical procedure is as following. Solution I was made by adding 5.4673 g C_{16}TMABr in 14 ml distilled water with stirring. 3.3964 g sodium silicate was dissolved in 7.5654 g distilled water to make solution II. The solution III was prepared by dissolving 0.1517 g $VOSO_4 \cdot 5H_2O$ in 15 ml distilled water. Solutions I and II were mixed together with vigorous stirring for 10 min. Solution III was then added slowly over a period of 30 min with stirring. The pH value was adjusted to 10 with 1.0 M H_2SO_4. The resulting gel was loaded into a Teflon-lined stainless-steel autoclave and kept at 150°C for 48 h. The resulting solid products were recovered by centrifugation, filtering, washing with deionized water and drying in air at 100°C. The dried product was then calcined at 450, 550 and 650°C for 6 h, respectively, to obtain calcined samples. Samples are designated as V-MCM(x)-z where x is the ratios of Si/V, and z is the calcination temperature. For example, V-MCM(30)-550 represents the MCM-41 sample with Si/V atomic ratio of 30 and was calcined at 550°C.

XRD

XRD analysis was conducted on a computer-controlled Siemens D500 diffractometer employing nickel-filtered Cu Kα radiation ($\lambda = 1.5418$ Å). The X-ray tube was operated at 40 kV and 30 mA. Spectra were scanned at 0.02° step size and 1 sec step time from 1° to 8°. Fluorophologopite mica (Standard Reference Material 675, National Bureau of Standards) was used as an external standard in order to protect the detector from the high energy of the incident X-ray beam and to resolve a peak at low angles, narrower incident and diffracted beam slits were required in this work.

FTIR

The chemical structures of the samples were examined using FTIR (Bio-Rad Co., FTS-155) operated at a resolution of 2 cm^{-1}. The measurements were made on the samples mixed with KBr at 1:50 by weight. The range of scan was from 400 to 4000 cm^{-1}.

UV-Vis Absorption Spectroscopy

The diffuse reflectance UV-vis spectra were measured with a Varian Lary 5E spectrophotometer equipped with a 60 mm Hitachi integrating sphere accessory. Powder samples were loaded in a quartz cell with Suprasil windows, and spectra were collected in the 200–500 nm wavelength range against a quartz standard.

N_2 Sorption Measurement

Pore size, pore volume, and surface area of the sample were obtained from the analysis of nitrogen adsorption and desorption isotherms carried out at −196°C in a volumetric apparatus (Micromeritics Co., ASAP 2010). Sets of nitrogen adsorption-desorption isotherms were analyzed using a cylindrical mode and the Kelvin equation. The samples were outgassed at 350°C for 12 h until the vacuum pressure was below 0.1 mPa before measurements were performed.

Thermal Analysis (DTA and TGA)

Thermal properties of the samples were examined by TGA (Perkin Elmer TGA-7) and DTA (Perkin Elmer DTA-1700). The samples used for TGA and DTA were the dried products (100°C, 48 h). For both TGA and DTA experiments, the samples were heated in a flowing air at a heating rate of 5°C/min from 30 to 800°C.

Scanning Electron Microscopy (SEM)

The microstructure of the sample was examined using a field emission SEM (Hitachi S-800) operated at 200 kV.

The samples were deposited on a sample holder with an adhesive carbon foil and sputted with gold.

Transmission Electron Microscopy (TEM)

The sample was dissolved in water and became colloid in the water. The powders in the colloidal solution were deposited on a grid with a holy carbon copper film and rapidly transferred to a JEOL JEM-1200 EX II electron microscope operating at 100 kV.

Results and Discussion

Synthesis

A series of V-MCM-41 samples with various Si/V ratios were synthesized. The addition of vanadyl sulfate aqueous solution directly into the silica gel mixture resulted in phase separation and formation of free V_2O_5 because vanadyl sulfate could be rapidly hydrolyzed in a solution of silicate monomers. For better incorporation of vanadium into the MCM-41 framework, the vanadyl sulfate aqueous solution was added to the gel mixture drop by drop. The as-synthesized V-MCM-41 with various Si/V ratios show different colors from white to light green, even green, and the calcined V-MCM-41 show color from white to yellow, even orange after rehydrated (Table 1).

XRD

The XRD patterns of the samples (Fig. 1) feature distinct Bragg peaks in the range $2\theta = 1$–8°, which can be indexed to different *hkl* reflections, in good agreement with a patterns from a purely siliceous MCM-41 [1–3]. One can see peaks d_{100}, d_{110}, d_{200} and d_{210} (Table 2). These four peaks are definitely indexed on the hexagonal lattice of MCM-41. The intensities of the three peaks d_{110}, d_{200} and d_{210} decreased upon calcination and finally vanished at 650°C. The results could be explained by the fact that the hexagonal lattice was contracted upon calcination, as can be expected when organic cations were replaced by protons and adjacent silanol groups condense [51, 52]. Depending on the compositions of V-MCM-41, lattice contractions can be as high as 25%. The percentage of lattice contraction for the sample 20-MCM is 11% as the sample calcined at 450°C, 12–16% when the sample was calcined at 550°C, and greater than 20% when the sample was calcined at 650°C. The absence of XRD peaks above 10° 2θ indicates that the atomic arrangement within the mesopore walls is disordered.

While the precise structure of the vanadium-containing silicate matrix was unknown, the presence of similar distinct reflectance in the XRD patterns suggests the presence of long range order in the framework of V-MCM-41, similar to that in siliceous MCM-41. Most of previous works [40–42] reported

Table 1. Color of V-MCM-41.

Samples (Si/V ratios)	As-synthesized	Calcined	Rehydrated
Si-MCM-41	White	White	White
V-MCM (34)	White	White	Light yellow
V-MCM (31)	Light green	White	Light yellow
V-MCM (29)	Light green	White	Light yellow
V-MCM (26)	Green	White	Yellow
V-MCM (13)	Green	White	Orange

Table 2. Miller index, d-spacing and unit cell parameter a_0 of V-MCM-41.

Samples (Si/V ratios)	d_{100} (nm)	d_{110} (nm)	D_{200} (nm)	d_{210} (nm)	d_{300} (nm)	a_0 (nm)
Si-MCM-41	4.29	2.42	2.09	1.57	1.19	4.95
V-MCM (34)	4.38	2.43	2.10	1.57	1.30	5.05
V-MCM (31)	4.50	2.47	2.15	1.61	1.34	5.09
V-MCM (29)	4.58	2.47	2.15	1.61	1.37	5.13
V-MCM (26)	4.59	2.49	2.17	1.63	–	5.20
V-MCM (13)	4.68	2.51	2.24	–	–	5.23

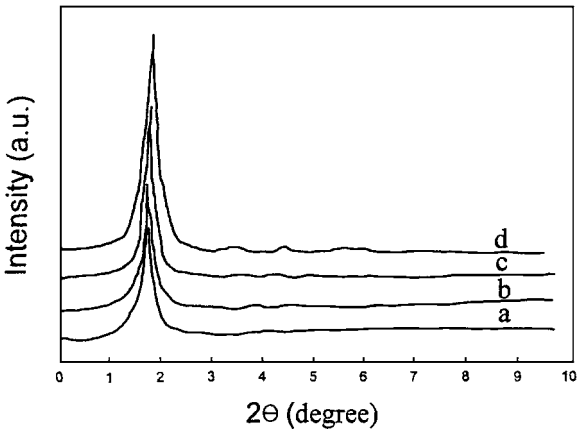

Figure 1. XRD spectra of V-MCM-41. (a) V-MCM (26), (2) V-MCM (29), (3) V-MCM (31), (d) V-MCM (34).

that V-MCM-41 should be synthesized at 150°C for 6 days. The results in this study show that 2 days were enough to get well-developed V-MCM-41 structure.

TGA and DTA

TGA detects three significant weight loss steps in the temperature regions 50–150, 150–300, and 300–450°C (Fig. 2). Mass spectroscopy reveals that only water was removed from the sample below 150°C. The endothermic peak near 100°C in DTA spectra (Fig. 3), assigned to water desorption, reconfirms this observation.

The weight loss between 150–450°C is accompanied by weak exotherms, indicating the combustion and decompositions of organic species (C_{16}TMABr surfactant) in air. The biomodal amine desorption probably results from the associatilon of $C_{16}H_{33}(CH_3)_3N^+$ with siloxy groups and Bronsted sites, the latter from vanadium [41]. The siloxy groups are stronger bases and should promote Hoffmann elimination at lower temperature [1]. The weight loss between 150–300°C is attributed to the dissociation of $C_{16}H_{33}(CH_3)_3N^+$ with SiO^- [1]. The weight loss between 300 and 450°C can be assigned to the dissociation of $C_{16}H_{33}(CH_3)_3N^+$ with VO^-. Two exothermic peaks appeared in DTA spectra reconfirm this conclusion [16, 24]. The as-synthesized sample contains about 50 wt% of organic species (Table 3) indicating that the as-synthesized sample contained large amount of organic surfactant due to the presence of mesoporous structure with large void volume. The TGA results also show that the sample with higher content of vanadium had a higher weight loss. The weight loss between 450–650°C is attributed to the loss of water via condensation of hydroxyl groups (Si—OH and V—OH) [16–24]. The weight loss levels off after 650°C. The results reveal that the surfactant can be removed upon calcination at 450°C. No exothermal peak after 450°C was observed in the DTA spectra, indicating that the surfactant has been removed completely.

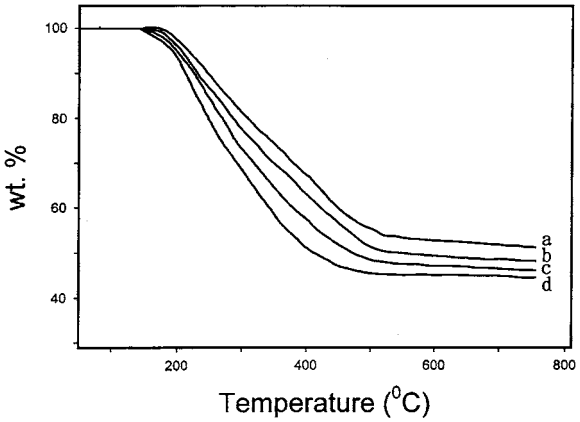

Figure 2. TGA spectra of V-MCM-41. (1) V-MCM (26), (2) V-MCM (29), (3) V-MCM (31), (4) V-MCM (34).

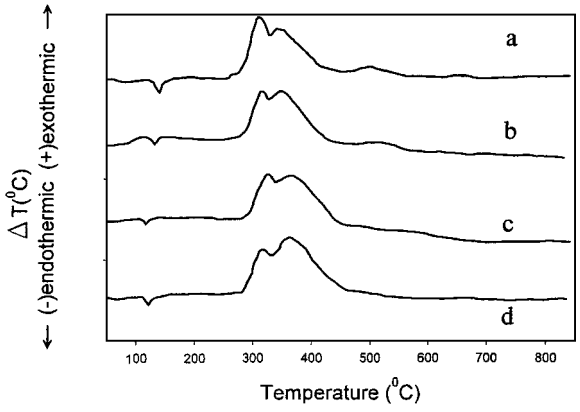

Figure 3. DTA plot. (a) V-MCM (26), (b) V-MCM (29), (c) V-MCM (31), (d) V-MCM (34).

Table 3. Weight loss of V-MCM-41.

Sample	Weight loss (wt%)	Weight loss (wt%)	Weight loss (wt%)
(Si/V ratio)	50–150°C	150–300°C	300–450°C
V-MCM (13)	2.56	35.21	7.36
V-MCM (26)	3.24	35.56	9.10
V-MCM (29)	3.65	36.97	9.98
V-MCM (31)	3.76	34.8	7.12
V-MCM (34)	4.12	33.9	8.23

Surface Area and Pore Size Distribution

The most reliable information about the mesoporous structure of solids comes from low-temperature N_2 adsorption-desorption isotherms. Figure 4 shows the typical result of nitrogen physisorbed at −196°C versus the relative pressure for sample V-MCM (31)-550. The isotherms are of type IV, typical of mesoporous solids. A well-defined step occurs between $p/p_o = 0.2$ and 0.3, which is indicative of the filling of the mesopore. The p/p_o coordinate of the inflection point depends on the pore size. The sharpness in this step

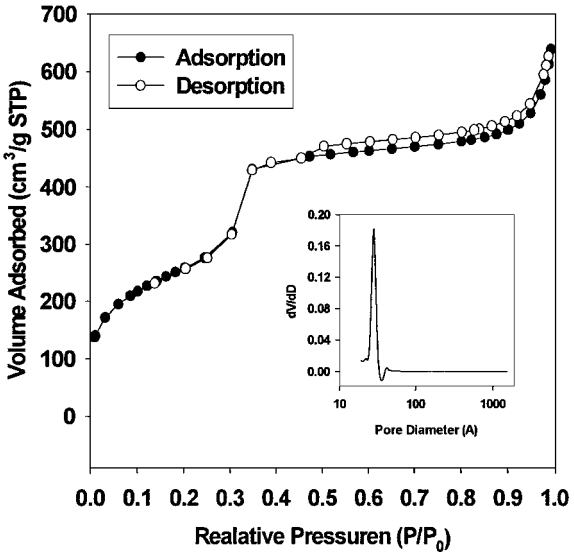

Figure 4. Nitrogen sorption results on V-MCM (31)-550.

suggests a uniform size pore system. The shape of the t-plot (not shown) appears to confirm that monolayer-multilayer adsorption has occurred on the pore walls before the onset of capillary condensation at $p/p_o = 0.2$. Furthermore, the fact that the initial region can be extrapolated back to the origin confirms the absence of any detectable micropore filling at low p/p_o. The large hysteresis loop at $p/p_o > 0.9$ indicates that the larger pores were filled at high relative pressures. This shows the formation of macropores upon calcination.

The isotherms contain an H_3 hysteresis loop as defined by IUPAC, associated with solids with slit-shaped pores or plate-like particles. Beck et al. [1] reported that the existance of slit-liked particles was formed. The SEM results in the latter section will show that the package of these plate-liked primary particles causes the existence of slit-liked pores. The capillary condensation inside the pores occurs when two lamellar adsorbed on the parallel walls touch each other, and fills the whole pore.

The BET surface area (Table 4) was calculated with the cross sectional area of a nitrogen molecule taken as 16.2 A^2. Incorporation of vanadium causes a decrease in BET surface area. The higher the vanadium content, the lower the BET surface area.

Although the desorption branch is often used for the assessment of the distribution of mesopore sizes, a type H_3 hysteresis loop is unlikely to yield a reliable estimate of pore size distribution, even for comparison purposes. Accordingly, the adsorption branch was used to calcu-

Table 4. BET surface area, pore volume and pore size of V-MCM-41.

Sample (Si/V ratio)	S_{BET} (m^2/g)	Pore size (A)
Si-MCM-41	1256	32.1
V-MCM (34)	1086	33.2
V-MCM (31)	1023	31.6
V-MCM (29)	929	32.8
V-MCM (26)	940	33.2
V-MCM (13)	685	32.9

late the mesopore size distribution. The typical plot of the derivative of the pore volume per unit weight with respect to the pore diameter (dV/dD) versus the pore diameter are shown in Fig. 4.

The BJH analysis for the physisorption of N_2 on the mesoporous materials give a remarkable narrow pore size distribution with a pore size of ca. 30 Å. The sharp pore size distribution, with a ca. 5 Å width at half-height, shows that the mesopores are very uniform. An additional peak is observed around 40 Å, possibly due to the nonuniform diameters in the channel. The pore diameters of the V-MCM-41 are listed in Table 5.

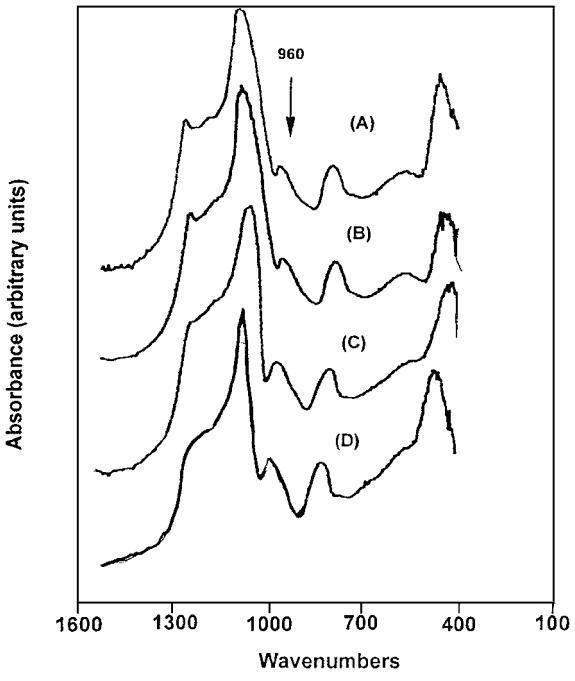

Figure 5. FTIR absorption spectra of V-MCM-41 with (a) V-free; (b) Si/V = 34; (c) Si/V = 26; (d) Si/V = 13.

FTIR

Infrared spectroscopy had been used extensively for the characterization of transition metal cations-modified zeolites. In the FTIR spectrum of calcined siliceous MCM-41, the asymmetric and symmetric stretching vibration bands of framework Si—O—Si bands, assigned by Sohn et al. [53] for zeolites, appeared at 1123 cm^{-1} and 814 cm^{-1}. In as-synthesized V-MCM these two bands appeared at somewhere lower wavenumbers, 1098 cm^{-1} and 802 cm^{-1}. After calcination to decompose the surfactant, these bands shifted to 1062 cm^{-1} and 796 cm^{-1}. In addition, the peak at 2780 cm^{-1} was assigned to the presence of surfactant. By the disappearing peak at 2780 cm^{-1}, one could conclude that the surfactant was completely decomposed. The results are in agreement with those in the literature [16].

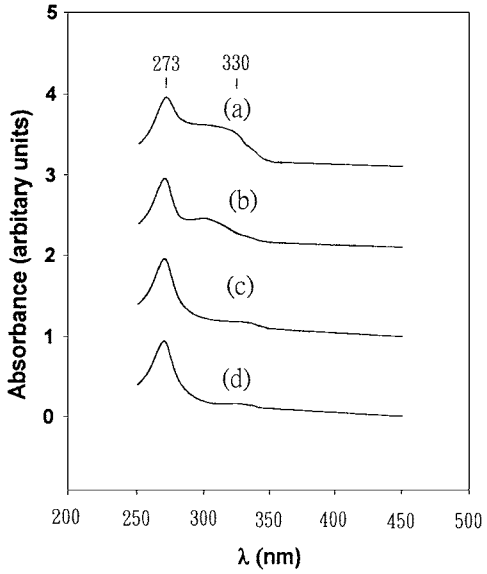

Figure 6. Diffuse reflectance UV-visible spectra of V-MCM-41 samples with (a) Si/V = 13; (b) Si/V = 26; (c) Si/V = 34; (d) V-free.

Table 5. Pore dimensions (nm) of V-MCM-41 materials.

Sample	d-spacing, d_{100} (nm)	Unit cell size, a_0 (nm)	Pore diameter, D (nm)	Wall thickness, T (nm)
Si-MCM-41	4.29	4.95	3.21	1.44
V-MCM (34)	4.38	5.05	3.32	1.73
V-MCM (31)	4.50	5.09	3.16	1.93
V-MCM (29)	4.58	5.13	3.28	1.85
V-MCM (26)	4.59	5.20	3.32	1.88
V-MCM (13)	4.68	5.23	3.29	1.94

D is internal pore diameter and t is wall thickness. a_0 is unit cell parameter, $t = a_0 - D$.

The FT-IR spectra of the V-MCM-41 with various compositions upon calcination at 550°C are shown in Fig. 5. On introduction of V, most of the bands were shifted to lower wavenumbers consistent with their incorporation in lattice positions. Additionally, an absorption band at ca. 960 cm^{-1} assigned to the vibration of Si—O—V linkages was observed. An FTIR band

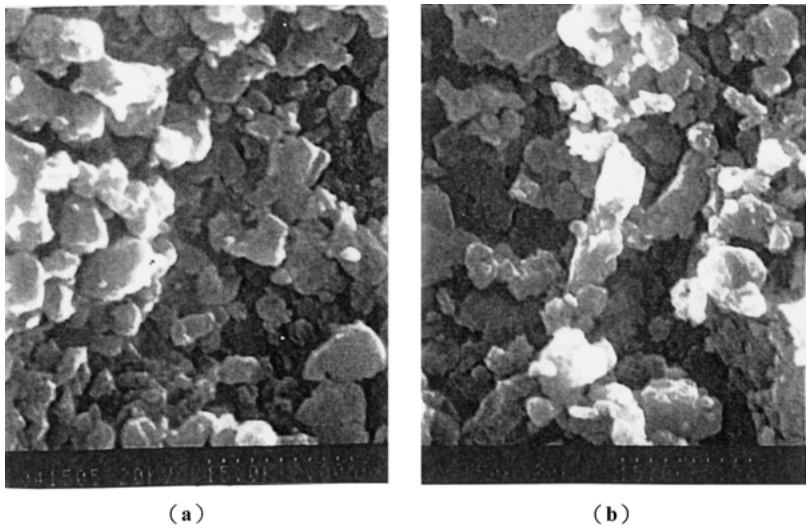

Figure 7. SEM images of V-MCM (31). (a) as-synthesized, (b) calcined at 550°C.

around 960 cm^{-1} was also observed in all samples. Such a band has been assigned to a stretching vibration mode of a [SiO_4] unit bonded to a titanium ion ($O_3Si{-}O{-}TiO_3$) in titanosilicate [19, 43] or to a vanadium ion ($O_3Si{-}O{-}VO_3$) in vanadosilicate molecular sieves [24]. This could be related to vanadium incorporation into framework positions. However, the origin and interpretation of this band are still in debate [19, 42]. Nevertheless, the ratio of the 960 cm^{-1} band in FTIR and the band at 800 cm^{-1} which is due to the symmetric stretching vibrations of SiO_4 was found to be significantly higher for V-MCM-41 samples than for siliceous MCM-41. It was inferred that the relative enhancement of the 960 cm^{-1} band may be attributed to vanadium incorporation. Park et al. [40] reported that V-MCM-41 having the Si/V ratio lower than 20 were completely collapsed after calcination. In this study, the sample with Si/V ratio of 13 was not collapsed after calcination.

UV-Vis

The V-MCM-41 samples with various compositions showed strong UV-vis absorption bands with overlapping maxima at 273 nm and 330 nm (Fig. 6). The relation between 273 nm and 330 nm seemed to have a

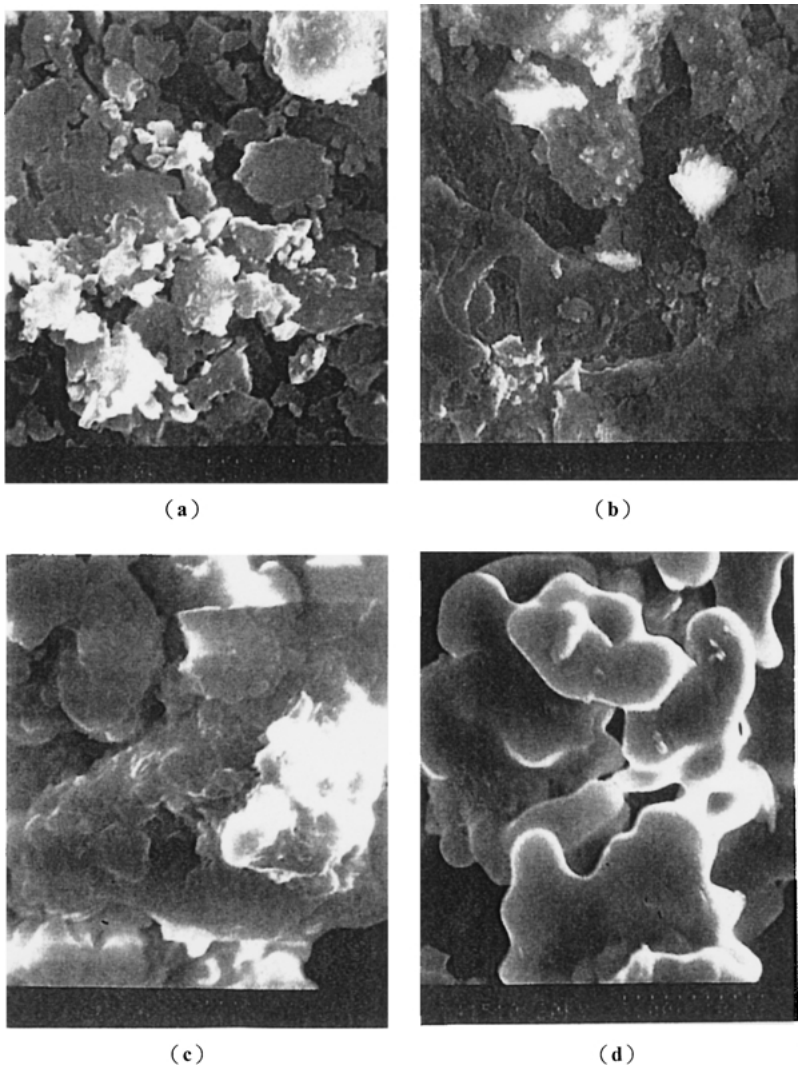

Figure 8. SEM images of V-MCM (31). (a) as-synthesized, (b) calcined at 450°C, (c) calcined at 550°C, (d) calcined at 650°C.

relatively higher intensity for higher vanadium loading. These bands were assigned to the low-energy charge transfer transitions between tetrahedral oxygen ligands and a central V^{5+} ion [24, 28]. Such a tetrahedral environment was typical for framework V^{5+} ions in zeolites [28] and was also found for some supported V_2O_5 catalysts [24]. Since the vanadium source added to the synthesis gel was a V^{4+} salt, the UV-vis results clearly indicated that most of the V^{4+} ions were oxidized to V^{5+} ions during synthesis.

Upon calcination in air, the V-MCM-41 samples changed from light green to white due to oxidation of small amount of VO^{2+} to V^{5+} ions. After exposure of these calcined samples to hydrated air, the color changed rapidly to bright yellow and then orange. This indicated additional coordination of water molecules to the V^{5+} ions. Based on these assignment, one can conclude that the charge transfer band at ca. 330 nm was attributable to V^{5+} ions with a short V═O double bond and three longer V─O bonds, possibly in interaction with water vapor [24, 31, 41, 42]. The 273 nm band was assigned to V^{5+} in a tetrahedral environment [28, 41, 42].

SEM

The SEM images are presented in Figs. 7 and 8. As one can see from the photos, the morphology is plate. It is relatively large in size, showing stepped and smooth surfaces. The big plate-agglomerate of the sample leads to a lower surface area inside the plates. Definitely, the surface area for fine dispersed spherical particles is larger than that for plates in close package. In addition, calcination had no influence on the morphology of the samples providing the temperature was less than 650°C. It should be noted that the morphology of siliceous MCM-41 is spherical shape as reported in the literature [1–3]. Incorporation of vanadium changed the morphology from sphere to plate.

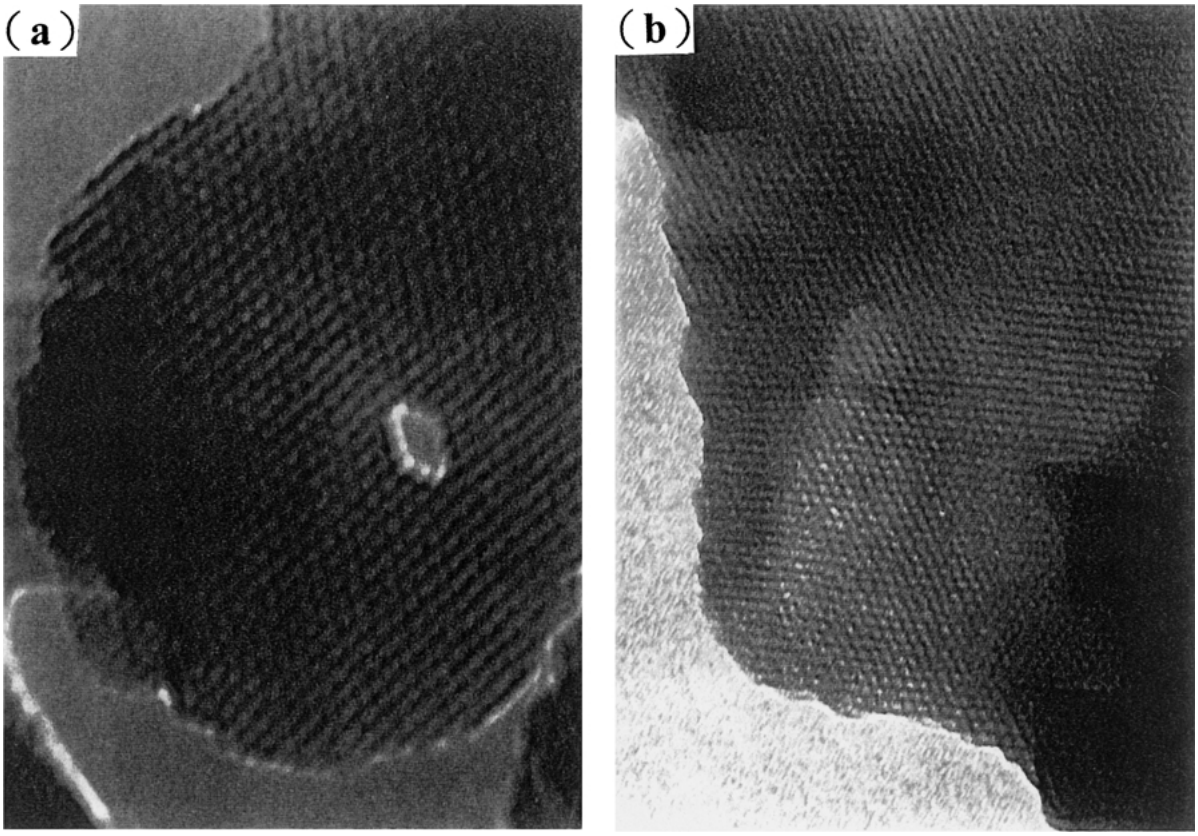

Figure 9. TEM images of V-MCM (31) (a) viewed down the pore axis at magnification, (b) viewed in the direction perpendicular to the pore axis.

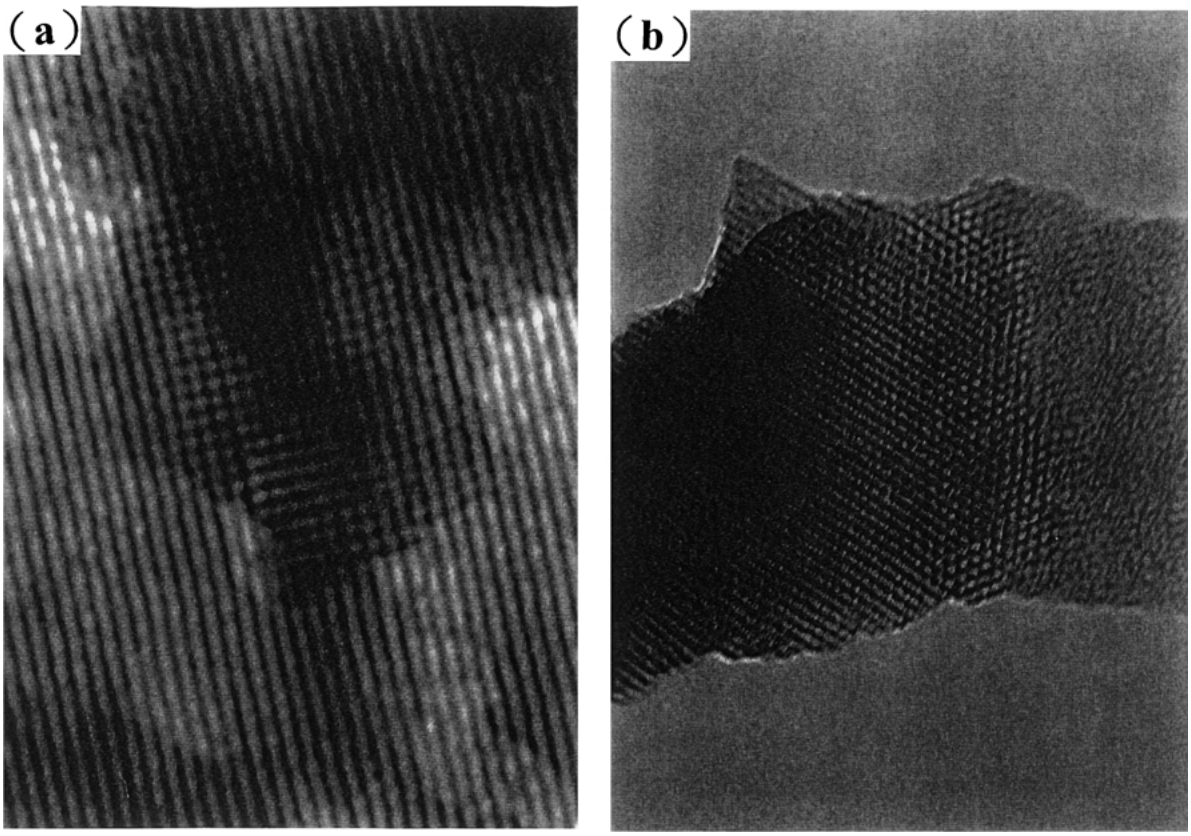

Figure 10. TEM images of V-MCM (31) viewed in the direction. (a) perpendicular to the pore axis, (b) down the pore axis.

TEM

Transmission electron micrographs viewed down the pore axis in Fig. 9 reveal a regular hexagonal array of uniform channels in a hexagonal arrangement. The repeat distance between the channels is about 40 Å, which is in excellent agreement with the position of the first peak in the XRD patterns. From TEM, the size of the pore is around 30 Å, the thickness of the pore wall was around 10 Å, and no order can be observed in the inorganic structure. When view in the direction perpendicular to their axis in Fig. 10, the pores are seen to be arranged in patches composed of regular rows more than 40 Å long. The morphology of MCM-41 tubules can be rectilinear. The pore size from Fig. 10 is ca. 35 Å in diameter. This is entirely consistent with the XRD and N_2 sorption results. The spacing between the neighboring rows in Fig. 10 is ca. 31 Å, which is related to the ca. 35 Å distance between pore centers by the factor of $\sqrt{3}/2$. Chenite et al. [54] have report that the interline distance of projection of a hexagonal array of tubules is related to the distances between pore centers by the same factor, and confirms that these lines are images of hexagonal tubes and not of the lamellar phase. There are virtually regular hexagonal arrays of fine pore arrangement existing in these samples. Besides, other workers [49, 51] found that samples which display only the (100) diffraction peak have very poorly organized pore system. One can conclude that incorporation of vanadium into the framework of MCM-41 affects the long-range order of the mesopores without damaging synthesized sample.

Conclusion

A series of V-MCM-41 mesoporous materials with various compositions have been synthesized. These samples were characterized with XRD, TGA, DTA, FTIR, UV-vis, N_2 sorption, SEM and TEM. The MCM-41 structure of the sample was confirmed by XRD. Vanadium was incorporated into the framework structure mainly in the tetrahedral site in the hydrated and

dehydrated samples. The concentration of octahedral site in the hydrated sample increased with an increase of vanadium content. The incorporation of vanadium in MCM-41 would decrease the regular order of structure to some extent. However, the V-MCM-41 samples did not collapse after calcination even for the sample having the Si/V ratio up to 13. The surfactant could be removed upon calcination at 450°C. The pore sizes of each sample were distributed very narrow. However, the formation of macropore after calcination was observed. Incorporation of vanadium decreased the surface area. The morphology of V-MCM-41 was plate with stepped and smooth surfaces, instead of spherical particles. TEM reveals a regular hexagonal array of uniform channels with curved and rectilinear morphologies. The hexagonal array structure of uniform pore size was observed by TEM. It is proved that the pores were highly aligned.

References

1. J.S. Beck, J.C. Vartuli, W.J. Roth, M.E. Leonowicz, C.T. Kresge, K.D. Schmitt, C.T.W. Chu, D.H. Olson, E.W. Sheppard, S.B. McCullen, J.B. Higgins, and J.B. Schlenker, J. Am. Chem. Soc. **114**, 10834 (1992).
2. C.T. Kresge, M.E. Leonowicz, W.J. Roth, J.C. Vartuli, and J.S. Beck, Nature **359**, 710 (1992).
3. C.Y. Chen, H.X. Li, and M.E. Davis, Micro. Mater. **2**, 27 (1993).
4. D.M. Antonelli and J.Y. Ying, Curr. Op. Coll. Interf. Sci. **1**, 523 (1996).
5. M.E. Davis, Nature **364**, 391 (1993).
6. P.T. Tanev, M. Chibwe, and T.J. Pinnavaia, Nature **368**, 321 (1994).
7. C.J. Brink, Curr. Op. Solid State Mater. Sci. **1**, 798 (1996).
8. Q. Huo, D.I. Margolese, and G.D. Stucky, Chem. Mater. **8**, 1147 (1996).
9. Q. Huo, D.I. Margolese, U. Ciesla, D.G. Demuth, P. Feng, T.E. Gier, P. Sieger, A. Firouzi, B.F. Chmelka, F. Schuth, and G.D. Stucky, Chem. Mater. **6**, 1176 (1994).
10. A. Sayari, Chem. Mater. **8**, 1840 (1996).
11. M.A. Camblor, A. Corma, and A. Martinez, J. Chem. Soc., Chem. Comm. **589** (1992).
12. W.A. Carcalho, P.B. Varaldo, M. Wallu, and U. Schuchardt, Zeolites **18**, 408 (1997).
13. C.F. Cheng and J. Klinowski, J. Chem. Soc., Faraday Trans. **92**, 289 (1996).
14. C.F. Cheng, H. He, W. Zhou, J. Klinowski, J.A.S. Goncalves, and L.F. Gladden, J. Phys. Chem. **100**, 283 (1996).
15. C.F. Cheng, Z.H. Luan, and J. Klinowski, Langmuir **11**, 2815 (1995).
16. Y.W. Chen and Y.H. Lu, Ind. Eng. Chem. Res. **28**, 1893 (1999).
17. Y.W. Chen, K.K. Koh, and Y.M. Wang, J. Chin. Inst. Chem. Engrs. **31**, 123 (2000).
18. M.J. Climent, A. Corma, R. Guil-Lopez, S. Iborra, and J. Primo, J. Catal. **175**, 70 (1998).
19. A. Corma, T. Navarro, and J.P. Pariente, J. Chem. Soc., Chem. Commun. **147** (1994).
20. A. Corma, M.A. Camblor, P. Esteve, A. Martinez, and J. Perez-Pariente, J. Catal. **151**, 213 (1994).
21. A. Corma, V. Fornes, M.T. Navarro, and J. Perez-Pariente, J. Catal. **148**, 569 (1994).
22. H.P. Lin and C.Y. Mou, Science **273**, 765 (1996).
23. C.C. Liu, X.K. He, and Y. Wu, Catal. Lett. **36**, 263 (1996).
24. Z.H. Luan, J. Xu, H. He, J. Klinowski, and L. Kevan, J. Phys. Chem. **100**, 19595 (1996).
25. M.W. Maddox, J.P. Olivier, and K.E. Gubbins, Langmuir **13**, 1737 (1997).
26. A.D. Maria, A.I. Tocerro, and J. Klinowski, J. Chem. Soc., Faraday Trans. **92**, 849 (1996).
27. J.Y. Ying, C.P. Liu, C.P. Mehnert, and M.S. Wong, Angew. Chem. Int. Ed. **38**, 56 (1999).
28. M. Morey, A. Davidson, H. Eckert, and G.D. Stucky, Chem. Mater. **8**, 486 (1996).
29. K.M. Reddy and C. Song, Catal. Lett. **36**, 103 (1996).
30. J.S. Reddy, P. Liu, and A. Sayari, Appl. Catal. A: General **148**, 7 (1996).
31. K.M. Reddy, I. Moudrakovski, and A. Sayari, J. Chem. Soc., Chem. Commun. 1059 (1994).
32. Z.H. Luan, C.F. Cheng, W. Zhou, and J. Klinowski, J. Phys. Chem. **99**, 1018 (1995).
33. Z.Y. Yuan, S.Q. Liu, T.H. Chen, J.Z. Wang, and H.X. Li, J. Chem. Soc., Chem. Commun. 973 (1995).
34. A. Sayari, C. Danumah, I.L. Moudrakouski, K.I. Ratcliffe, J.A. Ripmeester, and K.F. Preston, J. Phys. Chem. **99**, 373 (1995).
35. A. Sayari, C. Danumah, and I.L. Moudrakovcki, Mater. Res. Soc. Symp. Proc. **371**, 81 (1995).
36. W. Zhang, J. Wang, P.T. Tanev, and T.J. Pinnavaia, J. Chem. Soc., Chem. Commun. 979 (1996).
37. L. Zhang and J.Y. Ying, Ceramics Processing **43**, 11 (1997).
38. A. Sayari and I.L. Moudrakovski, in *Synthesis of Porous Materials: Zeolites, Clays and Nanostructures*, edited by M. Ocelli and H. Kessler (Marcel Dekker, New York, 1997), p. 417.
39. S. Gontier and A. Tuel, Microporous Mater. **5**, 161 (1995).
40. D.H. Park, C.F. Cheng, and J. Klinowski, Bull. Korea Chem. Soc. **18**, 1 (1997).
41. K.J. Chao, C.N. Wu, H. Chang, L.J. Lee, and S.F. Hu, J. Phys. Chem. B **101**, 6341 (1977).
42. Z. Luan, J. Xu, H. He, J. Klinowski, and L. Kevan, J. Phys. Chem. **100**, 19595 (1996).
43. Z. Luan, P.A. Meloni, R.S. Czernuszewicz, and L. Kevan, J. Phys. Chem. B **101**, 9046 (1997).
44. D. Wei, H. Wang, X. Feng, W.T. Chueh, P. Ravikovitch, M. Lyubovsky, C. Li, T. Takeguchi, and G.L. Haller, J. Phys. Chem. B **103**, 2113 (1999).
45. D. Wei, W.T. Chueh, and G.L. Haller, Catal. Today **51**, 501 (1999).
46. S. Lim and G.L. Haller, Appl. Catal. A: General **188**, 277 (1999).
47. M. Chatterjee, T. Iwasaki, H. Hayashi, Y. Onodera, T. Ebina, and T. Nagase, Chem. Mater. **11**, 1368 (1999).
48. G. Grubert, J. Rathousky, G. Schulz-Ekloff, M. Wark, and A. Zukal, Microporous Mesoporous Mater. **22**, 225 (1998).

49. A.B.J. Arnold, J.P.M. Niederer, T.E.W. Nieben, and W.F. Holderich, Microporous Mesoporous Mater. **28**, 353 (1999).
50. G. Xiong, C. Li, H. Li, Q. Zin, and Z. Feng, J. Chem. Soc., Chem. Comm. 677 (2000).
51. J.C. Vartuli, K.D. Schmitt, C.T. Kresge, W.T. Roth, M.E. Leonowicz, S.B. McCullen, S.D. Hellring, J.S. Beck, J.L. Schlenker, D.H. Olson, and E.W. Sheppard, Chem. Mater. **6**, 2317 (1994).
52. Z.H. Luan, P.A. Meloni, R.S. Czernuszewicz, and L. Kevan, J. Phys. Chem. **101**, 9046 (1997).
53. J.R. Sohn, S.J. Decanio, J.H. Lunsford, and D.J. Odonnell, Zeolites **3**, 225 (1986).
54. A. Chenite, L.Y. Page, and A. Sayari, Chem. Mater. **7**, 1015 (1995).